Scientific Reports

https://doi.org/10.1038/s41598-026-68073-w

Article in Press

Proteomic remodeling of the chicken spleen during astrovirus infection reveals coordinated interferon activation and stromal restructuring

Received: 18 May 2026

Accepted: 19 August 2026

Published online: 26 August 2026

Cite this article as: Sajewicz-Krukowska J., Rożek W., Malinowska A. *et al.* Proteomic remodeling of the chicken spleen during astrovirus infection reveals coordinated interferon activation and stromal restructuring. *Sci Rep* (2026). https://doi.org/10.1038/s41598-026-68073-w

Joanna Sajewicz-Krukowska, Wojciech Rożek, Agata Malinowska & Katarzyna Domańska-Blicharz

Proteomic remodeling of the chicken spleen during astrovirus infection reveals coordinated interferon activation and stromal restructuring

Joanna Sajewicz-Krukowska[1*], Wojciech Rożek[1], Agata Malinowska[2], Katarzyna Domańska-Blicharz[1]

[1]Department of Virology and Viral Animal Diseases, National Veterinary Research Institute, 57 Partyzantów Avenue, 24-100 Puławy, Poland; joanna.sajewicz@piwet.pulawy.pl (J.S.-K.); wojciech.rozek@piwet.pulawy.pl (W.R); domanska@piwet.pulawy.pl (K.D.-B.)

[2] Mass Spectrometry Laboratory, Institute of Biochemistry and Biophysics PAS in Warsaw, 5A Pawińskiego Street, 02-106 Warsaw, Poland; esme@ibb.waw.pl (A.M.)

[*] Correspondence: joanna.sajewicz@piwet.pulawy.pl; ORCID: 0000-0002-8471-0231

Keywords: chicken astrovirus; white chick syndrome; spleen proteomics; interferon signaling; extracellular matrix remodeling; transcriptome-proteome integration

Abstract

Chicken astrovirus (CAstV) is associated with white chick syndrome (WCS), characterized by reduced hatchability, hypopigmentation, developmental delay, and increased early mortality. Although transcriptomic studies have provided insight into host responses to CAstV infection, protein-level mechanisms remain poorly understood. Here, we performed label-free quantitative proteomic profiling of spleens from CAstV-infected SPF White Leghorn chickens to characterize systemic host responses.

Spleens collected at 4 days post-infection were analyzed by nanoLC–MS/MS. Among 1,118 quantified proteins, 34 showed significant differential abundance ($q \leq 0.05$). Proteins with increased abundance formed a type I interferon–associated antiviral module, including IFI27L1 (ISG12), OASL, STAT1, MOV10, and IFITM1, consistent with innate antiviral activation. Proteins with reduced abundance were enriched for extracellular matrix and cytoskeletal regulators, including decorin, lumican, mimecan, and actin-associated proteins, suggesting remodeling of the splenic stromal microenvironment.

Integration with previously generated RNA-seq data demonstrated concordant transcript–protein induction of interferon-stimulated genes alongside discordant regulation of extracellular matrix, cytoskeletal, and metabolic proteins, suggesting the involvement of post-transcriptional regulatory mechanisms. Together, these findings reveal coordinated antiviral, stromal, and metabolic

responses in the spleen during CAstV infection and provide a proteomic framework for understanding systemic host responses associated with white chick syndrome.

Introduction

Chicken astrovirus (CAstV) is a small, non-enveloped, positive-sense RNA virus belonging to the family *Astroviridae*, genus *Avastrovirus*. Although originally described as a cause of mild enteric disease, accumulating evidence indicates that CAstV can establish systemic infection and induce complex pathological outcomes in poultry. In chickens, CAstV has been implicated in several economically significant syndromes, including runting–stunting syndrome, growth impairment, nephropathy, and the characteristic white chick syndrome (WCS). WCS is defined by reduced hatchability, delayed embryonic development, generalized hypopigmentation of down feathers, and increased early post-hatch mortality [1-6]. Despite its growing relevance in commercial breeding systems, the molecular mechanisms underlying WCS remain insufficiently understood.

Vertical transmission plays a major role in the spread of CAstV, enabling infection of embryos during late stages of development and contributing to the systemic and developmental character of the disease. The virus exhibits broad tissue tropism, with viral detection and pathology documented in the gastrointestinal tract, liver, kidneys, and immune-associated tissues [1-3]. Among these, the spleen represents a central organ for systemic immune coordination. Although structurally distinct from its mammalian counterpart, the avian spleen is the principal secondary lymphoid organ responsible for filtering blood-borne antigens, orchestrating innate and adaptive immune responses, and activating type I interferon signaling [7,8]. Its cellular heterogeneity, including macrophages, dendritic cells, B cells, and T cells, provides the capacity for dynamic regulation of immune activation and metabolic adaptation during infection [7].

Because of its pivotal immunological function, the spleen provides a sensitive physiological readout of systemic host responses. Viral infections in chickens are known to induce splenic remodeling associated with oxidative stress, extracellular matrix (ECM) reorganization, and metabolic adaptation [8-12]. These processes may be relevant to the systemic host response accompanying CAstV infection. Because WCS is characterized by profound developmental abnormalities, understanding systemic immune and metabolic responses may provide broader biological context for the disease, although the direct relationship between splenic remodeling and WCS pathogenesis remains unclear[1,2,13].

Previous transcriptomic studies performed on tissues derived from the same experimental CAstV infection demonstrated robust activation of type I interferon (IFN-I) signaling, accompanied by strong upregulation of interferon-stimulated genes (ISGs) and concurrent suppression of mitochondrial and translational pathways [5]. These findings demonstrated coordinated antiviral and metabolic responses. However, transcript-level data alone cannot determine whether these alterations translate into functional changes in protein abundance or capture regulatory processes occurring post-transcriptionally, including changes in protein stability, turnover, or localization.

Proteomic analysis provides a complementary layer of insight by directly quantifying protein abundance and post-translational regulation [14]. Label-free quantitative mass spectrometry enables high-depth profiling of complex tissues without isotopic labeling and is well-suited for investigating systemic host responses to infection [15]. Although proteomic studies have been performed for several avian viral infections, including avian influenza virus and infectious bursal disease virus, comparable analyses are lacking for CAstV infection. Consequently, the relationship between transcriptomic responses and protein abundance during CAstV infection remains unknown, highlighting the need for integrated multi-omics approaches [1,5,6].

This study focused on a single acute time point (4 days post-infection) to characterize the early systemic host responses to CAstV infection. Accordingly, we performed a discovery-based label-free quantitative proteomic analysis of the chicken spleen and integrated these findings with our previously generated transcriptomic dataset. The aim of this exploratory multi-omics approach was to identify biological processes associated with the early host response and to distinguish transcriptionally driven antiviral responses from proteomic changes that may reflect additional regulatory mechanisms.

Results

Overview of the spleen proteome following CAstV infection

High-resolution label-free LC–MS/MS analysis of chicken spleen samples generated a comprehensive proteomic dataset. Across all samples, 2,529 proteins were identified (each supported by ≥2 unique peptides, protein level FDR ≤ 1%). A complete list of identified proteins is provided in Supplementary File 1. After applying a quantitative presence filter requiring detection in at least 4 of 5 biological replicates within at least one experimental group, 1,118 proteins were retained for downstream quantitative analysis (Supplementary File 2). The peptide abundance matrix used for quantitative analysis is provided in Supplementary File 3.

Protein loading and MS signal intensities were comparable across biological replicates, while blank injections confirmed minimal LC carryover, indicating good analytical reproducibility. Principal component analysis (PCA) of the quantified proteome showed partial overlap between CAstV-infected and control samples, with a tendency toward separation along the first principal component (PC1), suggesting moderate differences in global protein abundance profiles between experimental groups (Figure 1).

Figure 1. Principal component analysis (PCA) of quantitative spleen proteomes from control and CAstV-infected chickens. Each point represents one biological replicate (n=5 per group). Light blue symbols indicate control samples, whereas dark blue symbols represent CAstV-infected chickens. Component 1 and Component 2 explain 15.6% and 12.6% of the total variance, respectively. Samples showed partial separation between experimental groups, with moderate overlap, indicating infection-associated differences in global protein abundance profiles.

Detection of CAstV RNA in spleen samples

To confirm CAstV infection in the spleen samples used for proteomic analysis, the presence of viral RNA was assessed by RT-qPCR. CAstV RNA was detected in all spleens collected from infected chickens (Ct mean ± SD: 32.52 ± 2.37), whereas all control samples were negative

(undetected). These results confirmed that the spleen samples from infected chickens used for proteomic analysis were CAstV-positive.

Differentially abundant proteins

Of the 1,118 proteins retained for quantitative analysis, 34 exhibited statistically significant differences in abundance between the CAstV-infected (CA) and control (K) groups ($q \leq 0.05$) and were classified as differentially abundant proteins (DAPs). One additional protein (F1P2A1) was detected exclusively in control samples and therefore was not included in the statistical analysis. The overall distribution of protein abundance changes is shown in the volcano plot (Figure 2). The complete list of these 34 DAPs, including protein identifiers, fold changes, and statistical parameters, is provided in Table 1 and Supplementary File 4.

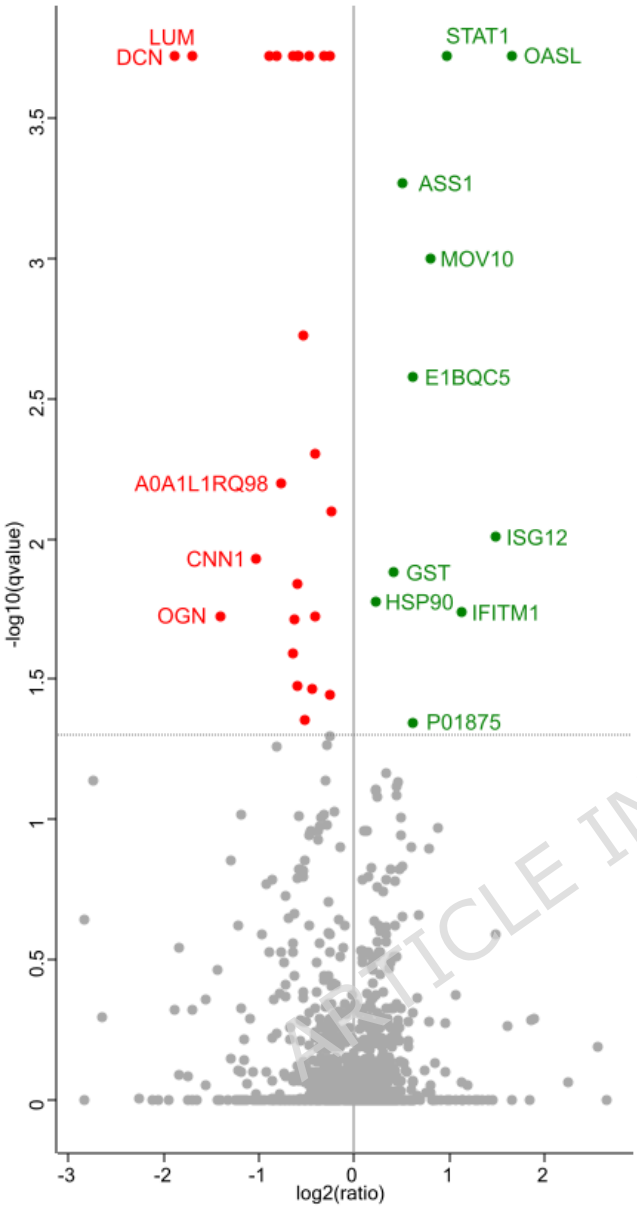

Figure 2. Volcano plot of differential protein abundance between CAstV-infected and control chicken spleen samples.

Each point represents one quantified protein (n = 1,118). The x-axis shows $\log_2$ fold change (CA/K), whereas the y-axis represents –log10(q-value). Green and red points indicate proteins with significantly increased and decreased abundance in CAstV-infected samples ($q \leq 0.05$), respectively. Selected differentially abundant proteins (DAPs) discussed in the text are labeled.

Among the 34 DAPs, 10 proteins showed increased abundance and 24 showed reduced abundance in the CA group relative to controls. Proteins with increased abundance were predominantly associated with the interferon response and included IFI27L1 (ISG12), OASL, STAT1, MOV10,

and IFITM1. Additional proteins with increased abundance comprised argininosuccinate synthase (ASS1), glutathione S-transferase (GST) and heat shock protein 90 (HSP90), suggesting activation of antiviral and cellular stress-response pathways.

Proteins with reduced abundance were mainly associated with extracellular matrix organization, cytoskeletal structure and cell adhesion. These included the extracellular matrix proteoglycans decorin (DCN), lumican (LUM), mimecan (OGN), together with several cytoskeleton- and adhesion-associated proteins or protein groups, including MYH10, MYH11, TAGLN, ACTA family proteins (including ACTA1), ACTN1/ACTN2, LPP, VCL, FERMT2, SPTBN1, and CNN1. Reduced abundance was also observed for the metabolic proteins, including ALDH6A1 and BSG.

To further characterize the biological significance of the identified DAPs, functional enrichment and protein-protein interaction analyses were performed.

Table 1. Differentially abundant proteins (DAPs) identified following CAstV infection

Differentially abundant proteins (DAPs) identified by label-free LC–MS/MS analysis of chicken spleen samples following CAstV infection are shown. Relative protein abundance (calculated as median of peptide ratios) is expressed as the CA/K ratio. The "Peptides" column indicates the number of peptides used for quantification of each protein or protein group. Proteins were considered differentially abundant at an adjusted q value ≤ 0.05. Where protein groups were identified, the leading UniProt identifier is shown, whereas the corresponding gene symbol reflects the protein group annotation. The complete protein group composition is provided in Supplementary File 4. F1P2A1 was detected exclusively in control samples and is shown separately because statistical testing could not be performed.

Protein (UniProt ID)	Gene symbol	Ratio CA/K	$\log_2$(ratio CA/K)	Q value	Peptides	Regulation
F1P2A1	–	only in K		–	2	Down
H9L0X6	OASL	3,14	1,65	0.00019	13	Up
Q5ZJK3	STAT1	1,97	0,98	0.00019	22	Up
E1BR38	ASS1	1,43	0,52	0.00054	14	Up
Q5ZKD7	MOV10	1,75	0,81	0.00184	12	Up
E1BQC5	–	1,54	0,62	0.00321	14	Up
Q6IEC5	ISG12	2,79	1,48	0.01005	5	Up
Q08392	GST	1,33	0,41	0.01190	9	Up
A0A1L1RND0	HSP90	1,17	0,23	0.01616	35	Up
R4GJX3	IFITM1	2,20	1,14	0.01807	3	Up
P01875	–	1,54	0,62	0.04302	9	Up
A0A1D5PH79	LOC107049991	0,57	-0,81	0.00019	15	Down

A0A1D5NUE9	MYH10	0,67	-0,58	0.00019	42	Down
P19966	TAGLN	0,54	-0,89	0.00019	11	Down
A0A1D5NW68	ALB	0,72	-0,47	0.00019	61	Down
A0A1D5P287	MYH11	0,80	-0,32	0.00019	108	Down
A0A1L1RX77	DCN	0,27	-1,89	0.00019	11	Down
P51890	LUM	0,31	-1,69	0.00019	8	Down
P68139	ACTA family (including ACTA1)	0,64	-0,64	0.00019	20	Down
A0A1D5P9P3	ACTN1/ACTN2	0,84	-0,25	0.00019	41	Down
Q5F464	LPP	0,66	-0,60	0.00019	12	Down
A0A3Q2TV38	–	0,69	-0,54	0.00218	13	Down
E1BT93	–	0,75	-0,42	0.00536	19	Down
A0A1L1RQ98	–	0,59	-0,76	0.00675	7	Down
P12003	VCL	0,85	-0,23	0.00713	51	Down
A0A452J7Z6	CNN1	0,49	-1,03	0.01146	6	Down
Q9W6H0	OGN	0,38	-1,40	0.01664	7	Down
A0A0A0MQ61	–	0,66	-0,60	0.01675	5	Down
E1C0T6	FERMT2	0,75	-0,42	0.01802	12	Down
F1P1L8	–	0,65	-0,62	0.02106	8	Down
F1NVF3	–	0,64	-0,64	0.02307	12	Down
P17790	BSG	0,66	-0,60	0.03267	5	Down
E1BQC2	Gal d 3	0,74	-0,43	0.03313	32	Down
E1C155	ALDH6A1	0,70	-0,51	0.03495	6	Down
A0A1D5P797	SPTBN1	0,84	-0,25	0.03516	90	Down

Proteins are ordered according to direction of regulation and ascending q-value.

Functional enrichment analysis of DAPs

Functional enrichment analysis demonstrated that the identified DAPs formed two functionally distinct groups. The first group comprised proteins associated with type I interferon–related antiviral responses, including IFI27L1 (ISG12), OASL, STAT1, MOV10, and IFITM1, all of which showed significantly increased abundance in CAstV-infected spleens. Although these proteins formed a biologically coherent antiviral module, their limited number precluded the identification of significantly enriched Gene Ontology (GO) terms or KEGG pathways by g:Profiler.

The second group comprised proteins involved in extracellular matrix organization, cytoskeletal structure, and cell adhesion, all of which showed reduced abundance in the CA group. This group included small leucine-rich proteoglycans decorin (DCN), lumican (LUM), and mimecan (OGN), as well as multiple cytoskeleton- and adhesion-associated proteins or protein groups such as calponin-1 (CNN1), myosin heavy chain proteins MYH10 and MYH11, transgelin (TAGLN), alpha-actin family proteins (including ACTA1), alpha-actinin 1/alpha-actinin 2 (ACTN1/ACTN2), lipoma-preferred partner homolog (LPP), vinculin (VCL), fermitin family member 2 (FERMT2), and spectrin beta chain (SPTBN1).

Functional enrichment analysis revealed a strong overrepresentation of terms related to structural organization terms, including actin filament binding (GO:0051015), actin cytoskeleton organization (GO:0030036), focal adhesion (GO:0048041), sarcomere (GO:0030017), Z-disc (GO:0030018), and muscle fiber contractile structures. KEGG and Reactome analyses further identified pathways related to actomyosin regulation and smooth muscle contraction (Figure 3). A detailed term-protein association map is provided in Supplementary File 5.

Protein–protein interaction (PPI) analysis performed using STRING further supported the functional organization of the identified DAPs. The interaction network revealed two major interconnected clusters (Figure 4). One cluster comprised interferon-stimulated antiviral proteins, including IFI27L1 (ISG12), OASL, STAT1, MOV10, and IFITM1. The second cluster consisted of extracellular matrix components (DCN, LUM, OGN) together with cytoskeletal and adhesion-associated proteins [CNN1, MYH10, MYH11, TAGLN, ACTA family proteins (including ACTA1), ACTN1/ACTN2, VCL, FERMT2, and SPTBN1].

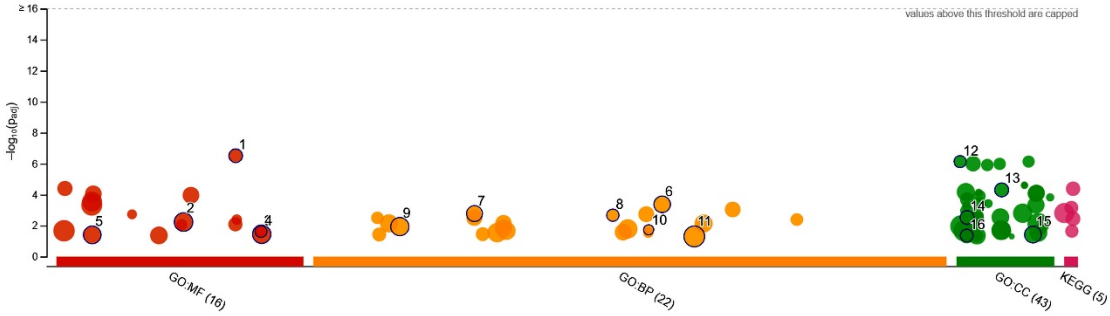

ID	Source	Term ID	Term Name	p_{adj} (query_1)
1	GO:MF	GO:0051015	actin filament binding	3.099×10^{-7}
2	GO:MF	GO:0043168	anion binding	5.883×10^{-3}
3	GO:MF	GO:0097110	scaffold protein binding	2.378×10^{-2}
4	GO:MF	GO:0097367	carbohydrate derivative binding	3.579×10^{-2}
5	GO:MF	GO:0005524	ATP binding	3.926×10^{-2}
6	GO:BP	GO:0060341	regulation of cellular localization	4.258×10^{-4}
7	GO:BP	GO:0030036	actin cytoskeleton organization	1.671×10^{-3}
8	GO:BP	GO:0048041	focal adhesion assembly	2.122×10^{-3}
9	GO:BP	GO:0009653	anatomical structure morphogenesis	1.157×10^{-2}
10	GO:BP	GO:0051900	regulation of mitochondrial depolarization	1.838×10^{-2}
11	GO:BP	GO:0065007	biological regulation	4.992×10^{-2}
12	GO:CC	GO:0001725	stress fiber	7.348×10^{-7}
13	GO:CC	GO:0043292	contractile muscle fiber	4.965×10^{-5}
14	GO:CC	GO:0005925	focal adhesion	2.976×10^{-3}
15	GO:CC	GO:0098590	plasma membrane region	3.776×10^{-2}
16	GO:CC	GO:0005903	brush border	4.326×10^{-2}

version	e113_eg59_p19_f6a03c19
date	29.10.2025, 11:05:43
organism	ggallus

g:Profiler

Figure 3. Functional enrichment analysis of differentially abundant proteins (DAPs).

Enrichment analysis was performed using g:Profiler. Significantly enriched Gene Ontology (GO) terms, including molecular function (MF), biological process (BP), and cellular component (CC), as well as KEGG pathways, are shown. Each point represents one enriched term, with the y-axis indicating statistical significance expressed as $-\log_{10}$(adjusted p-value). Enriched terms were predominantly associated with cytoskeletal organization, actin filament binding, focal adhesion, and contractile structures.

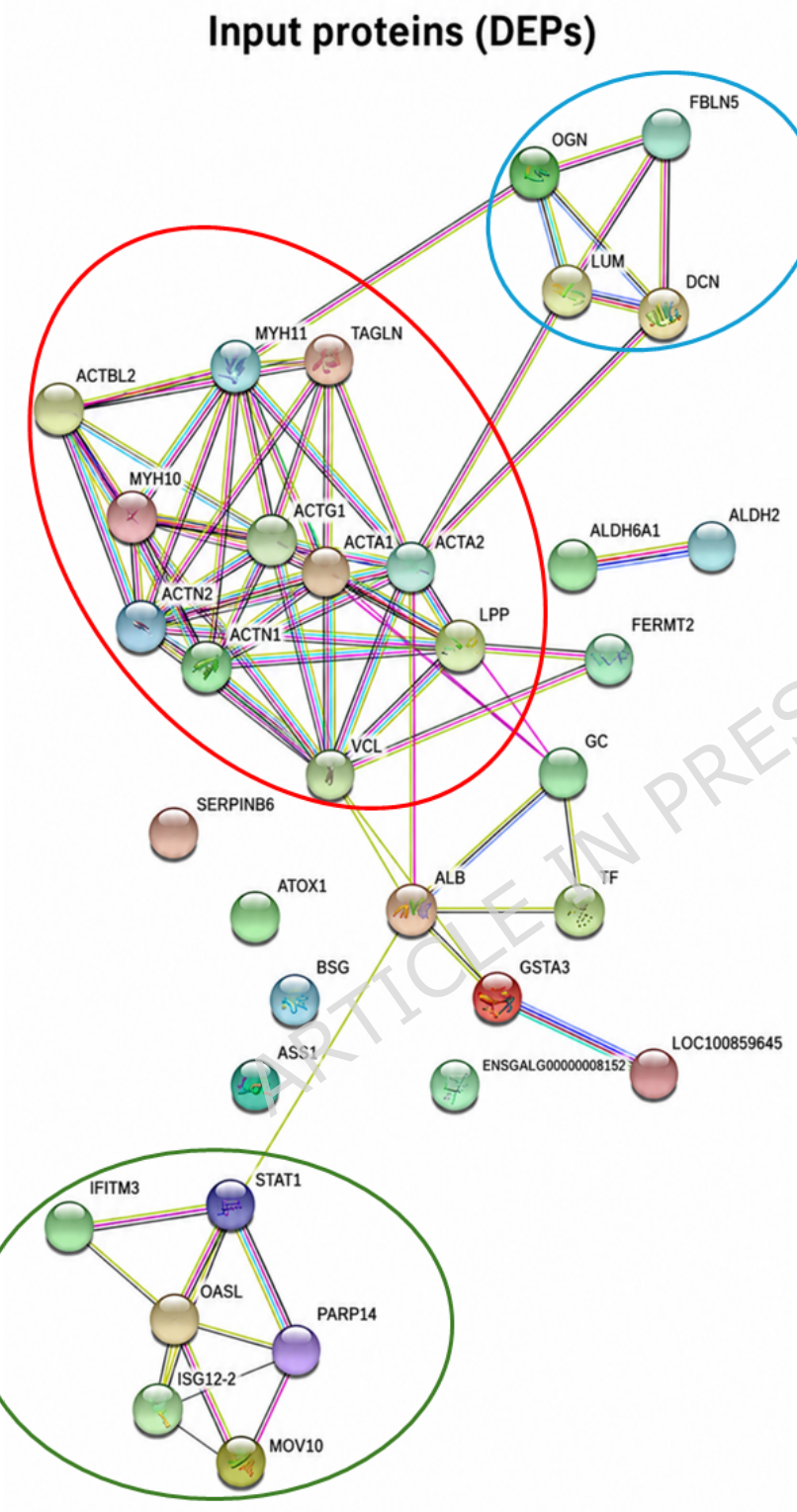

Figure 4. Protein–protein interaction (PPI) network of differentially abundant proteins (DAPs) identified in CAstV-infected spleens.

The network was generated using STRING v12.0 with a minimum interaction confidence score of 0.4 and includes only the identified DAPs. Nodes represent proteins, and edges indicate predicted or experimentally supported

interactions. Three major functional groups are highlighted: the green circle denotes the interferon-associated antiviral module (IFI27L1 /ISG12, OASL, STAT1, MOV10, and IFITM1), the blue circle indicates extracellular matrix (ECM) proteins (DCN, LUM, OGN), and the red circle highlights cytoskeleton- and adhesion-associated proteins involved in structural remodeling [CNN1, MYH10, MYH11, TAGLN, ACTA family proteins (including ACTA1) and ACTN proteins, VCL, LPP and FERMT2].

Extracellular matrix remodeling and structural reorganization

Several extracellular matrix (ECM)-associated proteins showed markedly reduced abundance in CAstV-infected spleens. Among the most strongly affected were the small leucine-rich proteoglycans (SLRPs) decorin (DCN), lumican (LUM) and mimecan (OGN), with CA/K abundance ratios of 0.27, 0.31, 0.38, respectively. In contrast, transcript levels of the corresponding genes in the previously generated RNA-seq dataset did not show comparable decreases. Reduced abundance was also observed for proteins involved in cell-matrix adhesion, including fermitin family member 2(FERMT2) and vinculin (VCL).

Together, these findings indicate coordinated remodeling of the extracellular matrix (ECM) and associated structural proteins at the proteome level that was not paralleled by corresponding transcriptional changes.

Interferon-stimulated protein induction

Several interferon-stimulated proteins exhibited increased abundance in CAstV-infected spleens. The strongest increase was observed for IFI27L1 (ISG12), followed by OASL, STAT1, MOV10 and IFITM1.

In contrast to the extracellular matrix-associated proteins, these interferon-stimulated proteins showed concordant regulation at both the transcript and protein levels, consistent with coordinated activation of the antiviral response.

Cytoskeletal remodeling

Several proteins involved in actin cytoskeleton organization, contractile structures, and cell adhesion showed reduced abundance in CAstV-infected spleens. Among these, calponin-1 (CNN1) exhibited one of the largest decreases (CA/K ratio=0.49). Reduced abundance was also observed for additional cytoskeleton- and adhesion-associated proteins, including myosin heavy chain 10 (MYH10), myosin heavy chain 11 (MYH11), transgelin (TAGLN), ACTA family proteins (including ACTA1), alpha-actinins (ACTN1/ACTN2), lipoma-preferred partner homolog (LPP), vinculin (VCL), fermitin family member 2 (FERMT2), and spectrin beta chain (SPTBN1). Functional enrichment analysis supported coordinated remodeling of cytoskeletal structures.

Significantly enriched Gene Ontology (GO) Cellular Component terms included *contractile muscle fiber* (GO:0043292), *sarcomere* (GO:0030017), *Z-disc* (GO:0030018), and *focal adhesion* (GO:0048041), together with Biological Process terms related to actin cytoskeleton organization and Molecular Function terms associated with actin filament binding. KEGG pathway analysis identified enrichment of *Vascular smooth muscle contraction* and *Regulation of actin cytoskeleton*, while Reactome analysis highlighted *Smooth Muscle Contraction*. Collectively, these findings indicate coordinated alterations of proteins involved in cytoskeletal organization and cell adhesion following CAstV infection.

Cross-omics comparison with RNA-seq data

Comparison of the proteomic dataset with previously published RNA-seq data [5], generated from the same biological samples and validated by RT-qPCR, revealed two distinct regulatory patterns **(**Figure 5; Supplementary File 6)**.** The first pattern reflected concordant transcript-protein regulation of interferon-associated genes. Proteins involved in type I interferon responses, including IFI27L1 (ISG12), OASL, STAT1, MOV10 and IFITM1, showed increased abundance at the protein level. Their corresponding transcripts exhibited the same direction of regulation, with OASL, STAT1 and MOV10 significantly upregulated (padj < 0.05)**,** whereas IFI27L1 and IFITM1 showed concordant but less pronounced transcript-level changes.

In contrast, the second regulatory pattern was characterized by protein-level alterations without corresponding transcriptomic changes. Extracellular matrix proteins, including DCN, LUM, OGN, together with cytoskeletal proteins, represented by calponin-1 (CNN1), exhibited reduced abundance at the protein level despite stable transcript abundance. A similar transcript-protein discrepancy was observed for additional cytoskeleton- and adhesion-associated proteins, including MYH10, MYH11, TAGLN, ACTA family proteins (including ACTA1), ACTN1/ACTN2, LPP, VCL, FERMT2 and SPTBN1.Overall, transcript and protein fold changes showed moderate concordance (Pearson r = 0.69; Spearman ρ = 0.58). The higher Pearson coefficient reflects agreement in the overall direction and magnitude of expression changes, whereas the lower Spearman coefficient indicates differences in the relative ranking of transcript and protein responses. This pattern is consistent with coordinated transcriptional regulation of interferon-associated genes together with post-transcriptional modulation of extracellular matrix, cytoskeletal, and selected metabolic proteins.

Overall, concordant transcript-protein regulation was primarily observed for interferon-associated genes, whereas extracellular matrix, cytoskeletal, and selected metabolic proteins displayed discordant regulation. These relationships are summarized in Figure 5, with the complete quantitative dataset provided in Supplementary File 6**.**

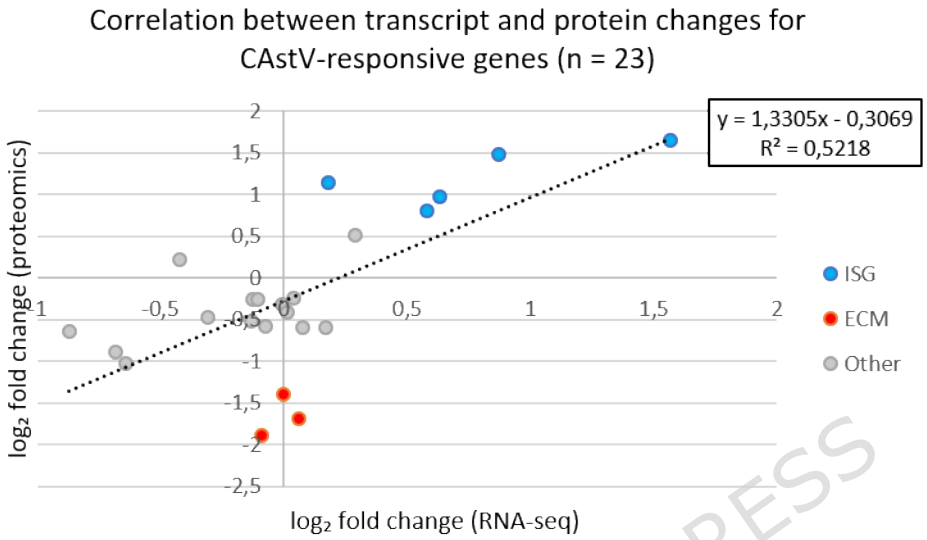

Figure 5. Cross-omics comparison of transcriptomic and proteomic responses to CAstV infection.

Each point represents one gene-protein pair quantified in both datasets. The x-axis shows transcriptomic $\log_2$ fold change (CA/K), and the y-axis shows proteomic $\log_2$ fold change (CA/K). Blue points indicate interferon-associated proteins, red points indicate extracellular matrix (ECM)-associated proteins, and grey points represent all remaining quantified gene-protein pairs. Only proteins with corresponding transcriptomic data (23 of the 34 DAPs) were included in the analysis. The solid line represents the linear regression fit, with the corresponding regression equation and coefficient of determination (R^2) shown. Overall concordance between transcriptomic and proteomic datasets is indicated by the Pearson ($r = 0.69$) and Spearman ($\rho = 0.58$) correlation coefficients.

Discussion

To our knowledge, this study provides the first quantitative proteomic characterization of the chicken spleen following infection with a chicken astrovirus (CAstV) strain associated with white chick syndrome (WCS). Among the 1,118 quantified proteins, 34 exhibited significant differential abundance, indicating that CAstV induces a selective rather than a global proteome-wide response. These proteomic alterations primarily involved antiviral signaling, extracellular matrix and cytoskeletal organization, and metabolic processes.

The proteomic data indicate activation of type I interferon–mediated antiviral responses in the spleens of CAstV-infected chickens. Several interferon-stimulated proteins (ISGs), including IFI27L1 (ISG12), OASL, STAT1, MOV10, and IFITM1, showed increased abundance.

Collectively, these proteins participate in antiviral defense by restricting viral replication and promoting innate immune signaling [16-18].

IFI27L1 and OASL are associated with interferon-mediated antiviral responses and modulation of RNA sensing pathways, and their increased abundance is consistent with the strong transcriptional induction previously observed in the same set of infected animals [5,19]. STAT1 is a canonical downstream mediator of JAK–STAT signaling, whereas MOV10 functions as an interferon-associated RNA helicase involved in antiviral defence. Together, these findings indicate that activation of the interferon response extends beyond transcriptional induction to the accumulation of antiviral effector proteins [20].

The increased abundance of IFITM1 is also consistent with activation of the antiviral response, as IFITM proteins inhibit viral entry and membrane fusion, thereby limiting infection at an early stage [21,22]. Detection of IFITM1 at the protein level is in agreement with the previously reported transcriptomic upregulation of IFIT family genes, although other IFIT proteins were not detected in the proteome, possibly reflecting their low basal abundance and rapid turnover [23,24].

Although the number of interferon-associated proteins among the DAPs was relatively small, their coordinated regulation and coherent functional profile support activation of a canonical type I interferon antiviral program [8,18]. Together, these findings indicate that CAstV infection induces a transcriptionally driven antiviral response that is reflected at the proteome level. Comparable activation of interferon-associated antiviral pathways has also been reported during proteomic analyses of avian influenza virus (AIV) infection, although the magnitude and composition of the induced protein repertoire depend on the virus subtype and infected tissue. Nevertheless, induction of innate immune effectors appears to represent a conserved feature of the avian antiviral response, supporting the conclusion that activation of type I interferon signaling constitutes a central component of the host response to CAstV infection [25].

Beyond activation of the interferon response, our proteomic analysis also revealed alterations in extracellular matrix (ECM) organization and stromal structural components.

One of the most prominent proteomic signatures in CAstV-infected spleens was the reduced abundance of the small leucine-rich proteoglycans (SLRPs) decorin (DCN), lumican (LUM), and mimecan (OGN). These proteins regulate collagen fibrillogenesis and contribute to the structural organization and mechanical properties of stromal networks [26,27]. Their coordinated reduction suggests active remodeling of the extracellular matrix during CAstV infection.

Importantly, transcript levels of DCN, LUM, and OGN remained unchanged in the corresponding RNA-seq dataset, suggesting that ECM remodeling may involve post-transcriptional mechanisms, including altered protein turnover or extracellular degradation, although additional regulatory mechanisms cannot be excluded. Similar extracellular matrix remodeling has been described in immune-activated stromal tissues, where increased protease activity contributes to matrix reorganization and immune cell migration [28,29]. Our findings are also broadly consistent with previous observations in other avian viral infections affecting the spleen. In particular, infectious bursal disease virus (IBDV) has been shown to induce marked disruption of splenic extracellular matrix organization, including degradation of collagen fibers and major extracellular matrix glycoproteins, resulting in altered tissue architecture and immune functions [30]. Although the underlying mechanisms differ between IBDV and CAstV infection, these observations further support the concept that extracellular matrix remodeling is a common feature of virus-induced pathology in avian lymphoid tissues.

Consistent with these observations, functional enrichment analysis highlighted structural terms including contractile muscle fiber, sarcomere, Z-disc, and focal adhesion. In addition, KEGG and Reactome analyses identified pathways related to actomyosin regulation, supporting coordinated remodeling of extracellular matrix and cytoskeletal organization during CAstV infection [28,31]. Reduced abundance of structural ECM components may increase stromal plasticity and facilitate immune cell migration during antiviral responses, as proposed for other immune-activated tissues [28-31].

SLRPs also contribute to developmental matrix patterning and pigment cell anchoring; therefore, their reduced abundance may represent one of several mechanisms contributing to the hypopigmentation phenotype characteristic of white chick syndrome [32].

Proteomic analysis also revealed reduced abundance of multiple cytoskeleton-associated proteins in CAstV-infected spleens, including calponin-1 (CNN1), myosin heavy chain proteins (MYH10, MYH11), transgelin (TAGLN), alpha-actin family proteins (including ACTA1), and alpha-actinin proteins (ACTN1/ACTN2). It should be noted that several of these entries represent protein groups identified on the basis of shared peptides. Therefore, the functional interpretation presented below refers to protein groups rather than unequivocally to individual protein isoforms. These proteins contribute to actin filament organization, contractile tension, focal adhesion dynamics, and cytoskeletal connectivity within stromal support cells that maintain splenic microarchitecture

[31,33,34]. Their coordinated reduction is consistent with decreased cytoskeletal tension and structural reorganization of the splenic stroma [31,34].

Functional enrichment analysis further supported these findings by identifying overrepresented terms related to contractile muscle fiber, sarcomere, Z-disc, and focal adhesion, together with KEGG and Reactome pathways associated with actomyosin regulation [28,31]. These results are consistent with coordinated remodeling of cytoskeletal organization during CAstV infection. Similar proteomic remodeling of host structural and stress-response pathways has been reported during other avian viral infections. Comparative proteomic analysis of tracheal tissues from chickens infected with infectious bronchitis virus (IBV), Newcastle disease virus (NDV), or avian influenza virus (AIV) H9 have also reported alterations in proteins involved in cytoskeletal organization, cell adhesion, and cellular metabolism, suggesting that structural reorganization is a common feature of the avian antiviral response. Nevertheless, the pronounced reduction of extracellular matrix proteoglycans observed during CAstV infection suggests that stromal remodeling may represent a particularly prominent component in this infection [35].

Similar cytoskeletal remodeling has been described in immune-activated tissues, where reduced actomyosin tension and increased structural plasticity are thought to facilitate immune cell migration and tissue adaptation during inflammatory responses [28,29,31,34]. Although the precise cellular mechanisms require further investigation, the observed proteomic changes are consistent with structural remodeling accompanying antiviral immune activation.

In addition to antiviral signaling and structural remodeling, CAstV infection was also associated with changes in proteins involved in intermediary metabolism.

CAstV infection was associated with reduced abundance of the mitochondrial enzyme aldehyde dehydrogenase 6 family member A1 (ALDH6A1), which participates in intermediary metabolism linked to tricarboxylic acid (TCA) cycle-associated pathways [36,37]. Although only a limited number of mitochondrial proteins met the threshold for differential abundance, the decrease in ALDH6A1 suggests localized modulation of mitochondrial metabolism during infection. Importantly, this reduction was not accompanied by corresponding changes in transcript abundance in the matching RNA-seq dataset, suggesting post-transcriptional regulation. Similar transcript–protein uncoupling has been described during antiviral responses, where mitochondrial enzymes are regulated through changes in protein stability, import, or turnover rather than transcriptional repression [10,11,23]. Even modest reductions in mitochondrial enzyme abundance

may reflect broader metabolic adaptation, as interferon signaling is known to limit biosynthetic activity while maintaining antiviral immune functions [10,38,39]. The reduced abundance of ALDH6A1 may therefore represent one component of this conserved metabolic response.

Together, these findings suggest that CAstV infection is accompanied by localized modulation of mitochondrial metabolism. Although based on a limited number of differentially abundant mitochondrial proteins, these observations are consistent with metabolic adaptations that have been described during antiviral responses [10,39].

CAstV infection was accompanied by protein-level changes indicative of active reorganization of the splenic microenvironment. Increased abundance of interferon-stimulated proteins together with reduced abundance of extracellular matrix proteoglycans and cytoskeletal proteins suggests coordinated remodeling of stromal architecture during antiviral responses. Similar patterns of stromal adaptation have been described in other immune-activated tissues [28,29].

Stromal cells are known to regulate immune cell positioning through dynamic changes in extracellular matrix composition and cytoskeletal organization [31]. Accordingly, the coordinated reduction of small leucine-rich proteoglycans (DCN, LUM, OGN) together with cytoskeletal proteins CNN1, MYH10, MYH11, TAGLN, ACTA family proteins (including ACTA1, ACTN1/ACTN2, VCL, FERMT2) is consistent with remodeling of the stromal microenvironment during antiviral immune responses [28,31,34].

Such remodeling may facilitate tissue adaptation during antiviral immune responses by increasing structural plasticity of the splenic microenvironment [28,29,31,34]. However, the precise cellular consequences of these proteomic changes remain to be determined.

Integration of the proteomic findings with previously generated transcriptomic data provided additional insight into the regulatory architecture underlying the host response to CAstV infection. Integration of the proteomic results with previously reported RNA-seq data revealed two mechanistically distinct layers of regulation associated with CAstV infection. Interferon-stimulated genes, including IFI27L1 (ISG12), OASL, STAT1, and MOV10 showed concordant increases at both transcript and protein levels, indicating that this antiviral response is predominantly transcriptionally driven. This pattern is consistent with canonical type I interferon activation, in which JAK–STAT signaling coordinates expression of antiviral effectors at both the mRNA and protein levels [5,20].

In contrast, proteins associated with extracellular matrix organization (DCN, LUM, OGN) and cytoskeletal organization [CNN1, MYH10, MYH11, TAGLN, ACTA family proteins (including ACTA1), ACTN1/ACTN2] exhibited reduced abundance without corresponding decreases in transcript levels. This divergence suggests that stromal remodeling may involve post-transcriptional regulatory mechanisms, including altered protein stability, turnover, or proteolytic processing, although additional regulatory mechanisms cannot be excluded [23,24,41]. A similar transcript-protein discrepancy was observed for the metabolic enzyme ALDH6A1, suggesting that metabolic remodeling during CAstV infection is likewise regulated at the protein level [10,39].

The moderate correlation between transcript and protein $\log_2$ fold-changes (Pearson $r = 0.69$; Spearman $\rho = 0.58$) further supports the presence of these two regulatory layers, as visualized in Figure 5. Interferon-stimulated genes showed strong concordance between transcript and protein abundance, whereas extracellular matrix proteins, cytoskeletal proteins, and ALDH6A1 displayed discordant transcript-protein relationships consistent with post-transcriptional regulation [42,43].

The characteristic hypopigmentation and growth impairment associated with white chick syndrome (WCS) may be related, at least in part, to the proteomic alterations observed during CAstV infection. The coordinated reduction of extracellular matrix proteoglycans (DCN, LUM, OGN) indicates remodeling of the splenic stromal microenvironment. Because SLRPs regulate collagen fibrillogenesis, extracellular matrix organization, and tissue architecture, their decreased abundance may represent one of several mechanisms contributing to developmental abnormalities associated with WCS [25,32]. Altered extracellular matrix organization has also been implicated in pigment-related developmental processes that depend on coordinated cell migration and tissue organization during embryogenesis [13].

The concurrent reduction of multiple cytoskeletal regulators, including CNN1, MYH10, MYH11, TAGLN, ACTA family proteins (including ACTA1), ACTN1/ACTN2, VCL, and FERMT2, further supports coordinated remodeling of stromal architecture during infection. Although the biological consequences of these alterations remain to be determined, changes in cytoskeletal organization could potentially influence tissue organization and developmental processes associated with WCS [13,40-42].

The reduced abundance of the mitochondrial metabolic enzyme ALDH6A1 suggests localized modulation of intermediary metabolism. Although only one mitochondrial protein met the threshold for differential abundance, alterations in metabolic pathways may influence energy-

demanding developmental processes and therefore could contribute to the complex pathogenesis of WCS [10,39,49]. However, this hypothesis requires further experimental validation.

Taken together, these findings indicate that CAstV infection induces two complementary regulatory layers in the chicken spleen: a predominantly transcriptionally driven interferon-mediated antiviral response and post-transcriptional remodeling of extracellular matrix organization, cytoskeletal architecture, and selected metabolic pathways. While antiviral responses showed good concordance between transcriptomic and proteomic data, structural and metabolic alterations were detected primarily at the protein level, emphasizing the importance of post-transcriptional regulation during CAstV infection. These findings highlight the value of integrative transcriptomic and proteomic analyses for understanding host responses to CAstV infection and provide a foundation for future studies investigating the molecular mechanisms underlying white chick syndrome.

Limitations

This study was conducted using five biological replicates per group, which is sufficient for detecting robust changes among moderately and highly abundant proteins but may limit the identification of low-abundance or transient regulatory factors. Additionally, label-free quantification measures relative protein abundance and cannot distinguish between altered protein synthesis, secretion, intracellular trafficking, or degradation. Although the coordinated decrease in extracellular matrix components suggests post-transcriptional remodeling, confirmation of the underlying mechanisms will require complementary approaches such as protease activity profiling, secretome analysis, and spatially resolved proteomics.

A further limitation of integrative transcriptomic-proteomic analyses is the frequently observed incomplete correspondence between mRNA abundance and protein levels, reflecting regulation at post-transcriptional, translational, and protein stability levels [24,41,44,45]. The moderate transcript-protein correlation observed in this study is therefore consistent with previous reports and most likely reflects biological regulation rather than technical variability.

Finally, while splenic proteome remodeling provides important insight into systemic host responses, direct analysis of skin and feather follicle tissues will be required to determine whether similar molecular alterations occur in tissues directly affected by the hypopigmentation and feather abnormalities characteristic of white chick syndrome.

Conclusions

This study provides the first high-resolution, label-free quantitative proteomic characterization of the chicken spleen during experimental infection with chicken astrovirus (CAstV) associated with white chick syndrome (WCS). A total of 2,529 proteins were identified, and 1,118 of them were quantified across biological replicates. Among these, 34 proteins exhibited significant differential abundance ($q \leq 0.05$), indicating that CAstV infection induces selective remodeling of the splenic proteome rather than widespread proteomic alterations.

The infection was associated with increased abundance of type I interferon-stimulated antiviral proteins, including IFI27L1 (ISG12), OASL, STAT1, MOV10 and IFITM1, supporting activation of a predominantly transcriptionally driven antiviral response. In contrast, extracellular matrix components, including the small leucine-rich proteoglycans decorin (DCN), lumican (LUM), and mimecan (OGN), were reduced in abundance despite stable transcript levels, indicating post-transcriptional regulation of ECM remodeling.

A coordinated decrease in cytoskeleton-associated proteins, including CNN1, MYH10, MYH11, TAGLN, ACTA family proteins (including ACTA1), ACTN1/ACTN2, LPP, VCL, FERMT2, and SPTBN1, is consistent with structural remodeling of the splenic microenvironment.

Metabolic alterations were also evident, most notably the reduced abundance of the mitochondrial enzyme ALDH6A1, suggesting post-transcriptional modulation of intermediary metabolism.

Integration of proteomic and transcriptomic data revealed two distinct regulatory layers: antiviral signaling was driven primarily at the transcriptional level, whereas extracellular matrix remodeling, cytoskeletal restructuring, and metabolic modulation occurred predominantly post-transcriptionally. Together, these findings demonstrate that antiviral signaling and structural remodeling are regulated through distinct molecular mechanisms during CAstV infection and provide a foundation for future studies investigating the molecular basis of white chick syndrome.

Overall, this study demonstrates the value of integrating proteomics with transcriptomics to identify regulatory mechanisms that cannot be resolved by transcriptomic analysis alone. Future studies incorporating metabolomics, spatial proteomics, and direct analysis of feather and skin tissues will further improve our understanding of the molecular mechanisms underlying white chick syndrome.

Materials and Methods

Experimental design and virus infection

The present study was conducted using the same experimental infection, animals, and spleen samples as those described previously by Sajewicz-Krukowska et al. [5]. Experimental conditions, virus propagation, inoculum preparation, and animal procedures were performed as previously described [5]. Briefly, the CAstV strain PL/G059/2014 (GenBank accession no. JF414802), associated with white chick syndrome, was propagated in embryonated specific pathogen free (SPF) chicken eggs.

SPF White Leghorn chicken eggs (VALO BioMedia, Osterholz-Scharmbeck, Germany) were incubated, hatched and housed in isolators until the chicks reached 21 days of age. Birds were then divided into two groups of five animals each (n=5 per group). The infected group was inoculated orally with 200 µl of the supernatant obtained after centrifugation of a 20% (w/v) homogenate of internal organs collected from PL/G059/2014-infected chicken embryos prepared in phosphate-buffered saline (PBS), whereas the control group received the same volume of sterile PBS.

Infection was initially confirmed by RT-qPCR analysis of cloacal swabs collected at 2 and 4 days post-infection (dpi) using the TaqMan assay described by Smyth et al. [46]. In addition, the presence of CAstV RNA was verified in the spleen samples used for proteomic analysis by RT-qPCR, as described below. At 4 dpi, all birds were humanely euthanized following sedation with isoflurane by decapitation. Spleens were aseptically excised, snap-frozen in liquid nitrogen, and stored at −80 °C until proteomic analysis.

Detection of CAstV RNA in spleen samples

To confirm the presence of CAstV RNA in the spleen samples used for proteomic analysis, approximately 30 mg of spleen tissue was homogenized using MP FastPrep homogenizer. Total RNA was isolated using RNeasy Mini Kit (Qiagen, Hilden, Germany) according to the manufacturer's instructions. Detection of CAstV RNA was performed using the same TaqMan RT-qPCR assay and reaction conditions as described above for cloacal swabs [46].

Protein extraction and sample preparation

Approximately 50–100 mg of spleen tissue from each sample was homogenized in lysis buffer (1% SDS, 30 mM Tris-HCl pH 8.0) using an MP FastPrep homogenizer. Lysates were cleared by centrifugation (14,000 × g, 20 min, 4 °C), and protein concentrations were determined using the Pierce BCA Protein Assay (Thermo Fisher Scientific).

For each sample, 100 µg of total protein was diluted to a final volume of 55 µl with urea buffer (8 M urea in 100 mM ammonium bicarbonate). Protein digestion was performed according to the filter-aided sample preparation (FASP) protocol with minor modifications [47]. Disulfide bonds were reduced by incubating with 50 mM tris (2-carboxyethyl) phosphine (TCEP) for 1 hour at 37°C, followed by transfer onto Vivacon 30 kDa molecular weight cut-off filters (Sartorius, Germany).

Samples were centrifuged at 14,000 x g for 30 min and washed twice with 200 µl of urea buffer. Cysteine residues were blocked by incubation with 100 mM S-methylmethanethiosulfonate (MMTS) for 15 min at room temperature. The filters were subsequently washed three times with urea buffer and three times with 100 mM ammonium bicarbonate to remove residual denaturant. After each washing step, samples were centrifuged for 15-40 min until the filters were dry. Proteolytic digestion was carried out overnight at 37°C with vortexing using 4 µg of Trypsin/Lys-C Mix (Promega) . Peptides were recovered from the filters by sequential centrifugation using 100 mM ammonium bicarbonate and 0.5 M sodium chloride. Peptide concentrations were measured using the Pierce Quantitative Colorimetric Peptide Assay (Thermo Fisher Scientific).

Mass spectrometry

A total of 2 µg of peptides from each sample was analysed using an LC-MS system consisting of a nanoUPLC chromatograph (nanoAcquity, Waters, Milford, MA, USA) directly coupled to a Q Exactive mass spectrometer (Thermo Fisher Scientific, Bremen, Germany). Samples were first loaded onto an RP-18 trap column (Waters, Milford, MA, USA) using water containing 0.1% formic acid (FA) and subsequently separated on an RP-18 analytical nano-HPLC column (75 µm x 250 mm, 1.7 µm particle size, Waters) using a linear gradient of 0–35% acetonitrile (ACN) in 0.1% FA over 160 min at a flow rate of 250 nL/min.

Mass spectra were acquired in data-dependent acquisition (DDA) mode. The twelve most intense precursor ions were selected for tandem mass spectrometry (MS/MS) using higher-energy collisional dissociation (HCD) with a normalized collision energy (NCE) of 27. Full MS scans were acquired over the m/z range of 300–1650 at a resolution of 70,000, with a maximum injection time of 60 ms and an automatic gain control (AGC) target of $1x10^6$ ions. MS/MS spectra were acquired with a maximum injection time of 60 ms, an AGC target value of $5x10^5$ ions, and an isolation window of 3.0 m/z. Dynamic exclusion was set to 30 s.

Blank injections and quality control (QC) samples were analyzed throughout the analytical sequence to monitor instrument stability and sample carryover.

Protein identification and label-free quantification

Raw MS data were searched in Mascot Server v2.8 (Matrix Science, London, UK) against the *Gallus gallus* reference proteome (UniProt release 2019_10, 27,542 sequences; 17,434,812 residues). Trypsin specificity was enforced with up to one missed cleavage allowed. Methylthio (C) was specified as a fixed modification, while methionine oxidation was included as a variable modification. Data were recalibrated offline, resulting in peptide and fragment mass tolerance of 5 ppm and 0.01 Da, respectively. Protein identifications were filtered to achieve a peptide-level false discovery rate (FDR) of ≤1%, estimated using a target-decoy strategy. Only proteins identified with at least two unique peptides were retained.

Mass calibration and data filtering were performed using the in-house MScan software, developed at the Institute of Biochemistry and Biophysics PAS [48].

For quantitative analysis, only proteins detected in at least four of five biological replicates within each experimental group were retained. LC peak volumes corresponding to monoisotopic peptide ions were extracted by overlaying the identified peptide list onto two-dimensional (2D) LC-MS heatmaps [49]. A total of 1,118 proteins fulfilled the inclusion criteria and were subjected to statistical analysis.

Differential abundance analysis was performed using the Diffprot algorithm with LOWESS normalization of quantitative values [50]. The normalized peptide abundance matrix used as the input for Diffprot is provided in Supplementary File 3. Proteins with more than 90% of shared peptides were clustered, resulting in 2404 clusters passed into further analysis and used in calculation of the correction for multiple-testing using the Benjamini-Hochberg procedure. Only cluster-unique peptides were used in statistical analysis. No missing values imputation was performed because the resampling-based Diffprot algorithm can accommodate missing values directly [50]. Proteins found in one group but not the other were excluded from statistical computations, with information on their presence in particular group given. Proteins with $q \leq 0.05$ were classified as differentially abundant proteins (DAPs). No additional fold-change threshold was applied.

Functional network analysis

Differentially abundant proteins (DAPs), identified using a q-value cutoff of ≤0.05, were subjected to functional enrichment analysis using g:Profiler [51]. The background set for enrichment analyses consisted exclusively of proteins identified in the LC-MS analysis rather than the complete *Gallus gallus* reference proteome. Functional enrichment was performed for Gene Ontology (GO) Biological Process (BP), Molecular Function (MF), and Cellular Component (CC) categories, as well as Kyoto Encyclopedia of Genes and Genomes (KEGG) and Reactome pathway annotations [52,53]. Statistical significance of enriched terms was assessed using FDR-adjusted p-values with a significance threshold of ≤0.05.

Protein–protein interaction (PPI) networks were examined using STRING v12.0 with a minimum interaction confidence score of 0.4 [54]. Only experimentally identified DAPs were included in the interaction network, and no additional first-shell interactors were added. The resulting network visualizations were used to identify functional clusters and interaction patterns among the differentially abundant proteins.

Cross-omic comparison and correlation analysis

Proteomic results were compared with previously generated RNA-seq data obtained from the same experimental CAstV infection and the same biological samples [5]. The RNA-seq dataset had been validated previously by RT-qPCR, allowing direct integration of transcriptomic and proteomic data derived from identical biological specimens.

For each differentially abundant protein (DAP), the corresponding gene-level $\log_2$ fold-change was retrieved when available. Cross-omics comparison was therefore restricted to proteins for which both proteomic and transcriptomic data were available. A total of 23 of the 34 DAPs met this criterion and were included in the correlation analysis.

Pearson's correlation coefficient was used to assess the linear relationship between transcript and protein $\log_2$ fold-changes, while Spearman's rank correlation coefficient was used to evaluate monotonic concordance. Correlation analyses were performed in Python [55].

Ethics statement

All animal experiments were performed in accordance with the European Union Directive 2010/63/EU on the protection of animals used for scientific purposes and were approved by the Local Ethics Committee for Animal Experiments at the University of Life Sciences in Lublin, Poland (Resolution No. 55/2019).

References

1. Smyth, V.J. A review of chicken astrovirus infections in chickens. *Avian Pathol.* **46(4)**, 384–391 (2017).
2. Raji, A.A., Omar, A.R. An Insight into the Molecular Characteristics and Associated Pathology of Chicken Astroviruses. *Viruses* **14(4)**, 722 (2022)
3. Sajewicz-Krukowska, J. et al. Astrovirus-induced "white chicks" condition - field observation, virus detection and preliminary characterization. *Avian Pathol.* **45(1)**, 2-12 (2016).
4. Sajewicz-Krukowska, J., Domanska-Blicharz, K. Nearly full-length genome sequence of a novel astrovirus isolated from chickens with 'white chicks' condition. *Arch. Virol.* **161(9)**, 2581-2587 (2016).
5. Sajewicz-Krukowska, J., Jastrzębski, J.P., Grzybek, M., Domańska-Blicharz, K., Tarasiuk, K., Marzec-Kotarska, B. Transcriptome Sequencing of the Spleen Reveals Antiviral Response Genes in Chickens Infected with CAstV. *Viruses* **13(12)**, 2374 (2021).
6. Sajewicz-Krukowska, J., Mirosław, P., Jastrzębski, J.P., Domańska-Blicharz, K., Tarasiuk, K., Marzec-Kotarska, B. miRNA Expression Signatures Induced by Chicken Astrovirus Infection in Chickens. *Int. J. Mol. Sci.* **24(20)**, 15128 (2023).
7. Fellah, J.S., Jaffredo, T., Dunon, D. Development of the avian immune system in *Avian Immunology* (ed. Davison, F., Kaspers, B., Schat, K.A.) 51-66 (London: Academic Press, 2008).
8. Le, T.T., Kim, T.H., Kwon, H.J. Type I interferon response in avian antiviral immunity. *Vet. Res.* **54**, 8 (2023).
9. O'Neill, L.A., Pearce, E.J. Immunometabolism governs dendritic cell and macrophage function. *J. Exp. Med*. **213(1)**, 15-23 (2016).
10. Mills, E.L., Kelly, B., O'Neill, L.A.J. Mitochondria are the powerhouses of immunity. *Nature Immunol.* **18**, 488–498 (2017).
11. Everts, B., Pearce, E.L. Metabolic control of dendritic cell activation and function: recent advances and clinical implications. *Front. Immunol.* **8**, 5, 203 (2014).
12. Hotamisligil, G.S. Foundations of immunometabolism and implications for metabolic health and disease. *Immunity* **47(3)**, 406–420 (2017).

13. Hirobe, T. How are proliferation and differentiation of melanocytes regulated? *Pigment Cell Melanoma Res.* **24(3)**, 462-478 (2011).
14. Aebersold, R., Mann, M. Mass-spectrometric exploration of proteome structure and function. *Nature* **537**, 347–355 (2016).
15. Cox, J., Mann, M. Quantitative, high-resolution proteomics for data-driven systems biology. *Annu. Rev. Biochem.* **80**, 273–299 (2011).
16. Fensterl, V., Sen, G.C. Interferon-induced IFIT proteins: their role in viral pathogenesis. *J. Virol.* **89(5)**, 2462-2468 (2015).
17. Schneider, W.M., Chevillotte, M.D., Rice, C.M. Interferon-stimulated genes: a complex web of host defenses. *Annu. Rev. Immunol.* **32**, 513–545 (2014).
18. McNab, F., Mayer-Barber, K., Sher, A., Wack, A., O'Garra, A. Type I interferons in infectious disease. *Nat. Rev. Immunol.* **15(2)**, 87–103 (2015).
19. Zhu, J., Ghosh, A., Sarkar, S.N. OASL-a new player in controlling antiviral innate immunity. *Curr. Opin. Virol.* **12**, 15-19 (2015).
20. Ivashkiv, L.B., Donlin, L.T. Regulation of type I interferon responses. *Nat. Rev. Immunol.* **14**, 36–49 (2014).
21. Bailey, C.C., Zhong, G., Huang, I.C., Farzan, M. IFITM-family proteins: the cell's first line of antiviral defense. *Annu. Rev. Virol.* **1**, 261–283 (2014).
22. Brass, A.L. et al. The IFITM proteins mediate cellular resistance to influenza A H1N1 virus, West Nile virus, and dengue virus. *Cell* **139(7)**, 1243–1254 (2009).
23. Vogel, C., Marcotte, E.M. Insights into the regulation of protein abundance from proteomic and transcriptomic analyses. *Nat. Rev. Gen.* **13(4)**, 227–232 (2012).
24. Maier, T., Güell, M., Serrano, L. Correlation of mRNA and protein in complex biological samples. *FEBS Letters* **583(24)**, 3966–3973 (2009).
25. Zou, W., Ke, J., Zhang, A., Zhou, M., Liao, Y., Zhu, J., Zhou, H., Tu, J., Chen, H., Jin, M. Proteomics analysis of differential expression of chicken brain tissue proteins in response to the neurovirulent H5N1 avian influenza virus infection. *J. Proteome Res.* **9(8),** 3789-98 (2010).
26. Iozzo, R.V., Schaefer, L. Proteoglycan form and function: A comprehensive nomenclature of proteoglycans. *Matrix Biol*. **42**, 11-55 (2015).

27. Kalamajski, S., Oldberg, Å. The role of small leucine-rich proteoglycans in collagen fibrillogenesis. *Matrix Biol.* **29(4)**, 248–253 (2010).
28. Mueller, S.N., Germain, R.N. Stromal cell contributions to the homeostasis and functionality of the immune system. *Nat. Rev. Immunol.* **9**, 618–629 (2009).
29. Rodda, L.B. et al. Single-cell RNA sequencing of lymph node stromal cells reveals niche-associated heterogeneity. *Immunity* **48(5)**, 1014–1028 (2018).
30. Bíró, E., Kocsis, K., Nagy, N., Molnár, D., Kabell, S., Palya, V., Oláh, I. Origin of the chicken splenic reticular cells influences the effect of the infectious bursal disease virus on the extracellular matrix. *Avian Pathol.* **40(2),** 199-206 (2011).
31. Chang, J.E., Turley, S.J. Stromal infrastructure of the lymph node and coordination of immunity. *Trends Immunol.* **36(1)**, 30–39 (2015).
32. Chen S, Birk DE. The regulatory roles of small leucine-rich proteoglycans in extracellular matrix assembly. *FEBS J.* **280(10)**, 2120-2137 (2013).
33. Gimona, M., Djinovic-Carugo, K., Kranewitter, W.J., Winder, S.J. Functional plasticity of calponin homology domains. FEBS Letters **513(1)**, 98–106 (2002).
34. Gunning, P.W., Hardeman, E.C., Lappalainen, P., Mulvihill, D.P. Tropomyosin – master regulator of actin filament function in the cytoskeleton. *J. Cell Sci.* **128(16)**, 2965-2974 (2015).
35. Sun, J., Han, Z., Shao, Y., Cao, Z., Kong, X., Liu, S. Comparative proteome analysis of tracheal tissues in response to infectious bronchitis coronavirus, Newcastle disease virus, and avian influenza virus H9 subtype virus infection. *Proteomics* **14(11),** 1403-23 (2014).
36. West, A.P., Shadel, G.S., Ghosh, S. Mitochondria in innate immune responses. *Nat. Rev. Immunol.* **11(6)**, 389–402 (2011).
37. Chandel, N.S. Evolution of mitochondria as signaling organelles. *Cell Metabol.* **22(2)**, 204–206 (2015).
38. O'Neill, L.A., Pearce, E.J. Immunometabolism governs dendritic cell and macrophage function. *J. Exp. Med*. **213(1)**, 15-23 (2016).
39. Thyrsted, J., Holm, C.K. Virus-induced metabolic reprogramming and innate sensing hereof by the infected host. *Curr. Opin. Biotechnol.* **68**, 44-50 (2021).

40. Gerner, M.Y., Torabi-Parizi, P., Germain, R.N. Strategically localized dendritic cells promote rapid T cell responses to lymph-borne particulate antigens. *Immunity* **42(1)**, 172-85 (2015).
41. de Sousa Abreu, R., Penalva, L.O., Marcotte, E.M., Vogel, C. Global signatures of protein and mRNA expression levels. *Mol. Biol. Syst*. **5(12)**, 1512–1526 (2009).
42. Haider, S., Pal, R. Integrated analysis of transcriptomic and proteomic data. *Curr. Genom.* **14(2)**, 91–110 (2013).
43. Perco, P., Mühlberger, I., Mayer, G., Oberbauer, R., Lukas, A., Mayer, B. Linking transcriptomic and proteomic data on the level of protein interaction networks. *Electrophoresis* **31(11)**, 1780–1789 (2010).
44. Randall, R.E., Goodbourn, S. Interferons and viruses: an interplay between induction, signalling, antiviral responses and virus countermeasures. *J. Gen. Virol,* **89(Pt 1)**, 1–47 (2008).
45. Greenbaum, D., Colangelo, C., Williams, K., Gerstein, M. Comparing protein abundance and mRNA expression levels on a genomic scale. *Genome Biol.* **4(9)**, 117 (2003).
46. Smyth, V.J., Jewhurst, H.L., Wilkinson, D.S., Adair, B.M., Gordon, A.W., Todd, D. Development and evaluation of real-time TaqMan RT-PCR assays for the detection of avian nephritis virus and chicken astrovirus in chickens. *Avian Pathol.* **39(6)**, 467–474 (2010).
47. Wiśniewski, J.R., Zougman, A., Nagaraj, N., Mann, M. Universal sample preparation method for proteome analysis. *Nat. Methods.* **6**, 359–362 (2009).
48. MScan software. Available online: *http://proteom.ibb.waw.pl/mscan/*
49. Bakun, M. et al. An integrated LC-ESI-MS platform for quantitation of serum peptide ladders. Application for colon carcinoma study. *Proteom Clin. Appl.* **3(8)**, 932–946 (2009).
50. Malinowska, A., Kistowski, M., Bakun, M., Rubel, T., Tkaczyk, M., Mierzejewska, J., Dadlez, M. Diffprot – software for non-parametric statistical analysis of differential proteomics data. *J. Proteom.* **75(13)**, 4062–4073 (2012).
51. g:Profiler. Available online: *https://biit.cs.ut.ee/gprofiler/index.cgi*.
52. The Gene Ontology Home Page. Available online: *http://geneontology.org/*
53. KEGG. Available online: *http://www.genome.jp/kegg/*

54. Szklarczyk, D. et al. The STRING database in 2023: protein–protein association networks and functional enrichment analyses for any sequenced genome of interest. *Nucleic Acids Res.* **51(D1)**, D638–D646 (2023).
55. Python. Available online: *https://www.programiz.com/python-programming/online-compiler*
56. Pérez-Riverol, Y. et al. The PRIDE database resources in 2022: a hub for mass spectrometry-based proteomics evidences. *Nucleic Acids Res.* **50(D1)**, D543–D552 (2022).

Author contributions

Conceptualization, J.S.-K.; methodology, J.S.-K.; validation, J.S.-K.; formal analysis, J.S.-K. A.M., W.R; investigation, J.S.-K. and A.M.; data curation, J.S.-K., A.M.; writing—original draft preparation, J.S.-K.; writing—review and editing, J.S.-K., A.M., W.R., K.D.-B., visualization, J.S.-K.; supervision, J.S.-K.; funding acquisition, J.S.-K. All authors have read and agreed to the published version of the manuscript.

Funding:

This research received no external funding.

Data Availability

The mass spectrometry proteomics data have been deposited to the ProteomeXchange Consortium via the PRIDE partner repository with the dataset identifier PXD074601 and 10.6019/PXD074601 [56]. The dataset will be made publicly available upon publication.

Competing interests

The authors declare no competing interests.

Supplementary information

The online version contains supplementary material available at …..